JGR Atmospheres

RESEARCH ARTICLE
10.1029/2020JD034355

The Dust Emission Potential of Agricultural-Like Fires—Theoretical Estimates From Two Conceptually Different Dust Emission Parameterizations

R. Wagner[1,2], K. Schepanski[2], and M. Klose[3,4]

[1]Leibniz Institute for Tropospheric Research (TROPOS), Leipzig, Germany, [2]Freie Universität Berlin (FU Berlin), Institute of Meteorology, Berlin, Germany, [3]Barcelona Supercomputing Center (BSC), Barcelona, Spain, [4]Now at Department Troposphere Research (IMK-TRO), Karlsruhe Institute of Technology (KIT), Karlsruhe, Germany

Key Points:

- Aerodynamic preconditions to favor dust emission through saltation and direct aerodynamic entrainment exist in fire vicinity
- Strength of relative contribution of both dust emission processes can vary significantly depending on wind, fire and soil-surface conditions
- Accurate estimation of global importance of fire-related dust emissions requires development of an adjusted parameterization approach

Correspondence to:
R. Wagner,
robert.wagner@tropos.de

Citation:
Wagner, R., Schepanski, K., & Klose, M. (2021). The dust emission potential of agricultural-like fires—Theoretical estimates from two conceptually different dust emission parameterizations. *Journal of Geophysical Research: Atmospheres*, *126*, e2020JD034355. https://doi.org/10.1029/2020JD034355

Received 17 DEC 2020
Accepted 30 AUG 2021

Abstract Agricultural fires affecting grass-, crop- and shrublands represent a major, mainly anthropogenically driven disturbance of many ecosystems. In addition to emissions of carbonaceous aerosol, they were found to inject also mineral dust particles into the atmosphere. The fires can significantly modulate the near-surface wind patterns so that conditions suitable for dust emission occur. However, the exact emission mechanism has not been investigated so far, but is inevitable for the understanding of its impacts on the Earth system. Here, we test two dust emission parameterizations representing saltation bombardment (SALT) and direct aerodynamic dust entrainment by (convective) turbulence (convective turbulent dust emission, CTDE) in the context of fire-modulated wind patterns using large-eddy simulation with an idealized setup to represent typical agricultural fire settings. Favorable aerodynamic preconditions for the initialization of both emission processes are found, however, with sometimes significant differences in dust emission flux depending on specific wind and fire properties. The strong fire-induced modulations of the instantaneous momentum flux suggest that CTDE can be a very potent emission process in the fire vicinity. Nevertheless, fire impacts on the friction velocity can be significant too, so that dust emission through SALT is facilitated as well. Ultimately, the specific aerodynamic conditions within pyro-convectively modulated wind patterns require the development of a parameterization that can describe these unique fire-related dust emissions and their influencing factors properly. This will finally allow for considering fire-induced dust emissions in aerosol-atmosphere models and an investigation of its atmospheric impacts such as on the radiation budget.

Plain Language Summary Mineral dust particles are frequently observed within smoke plumes originating from agricultural fires of mostly semi-arid regions. Such fires can modulate the near-surface wind patterns and thus foster dust emission. However, the exact emission mechanism has not been investigated so far. Here, two conceptually different dust emission parameterizations are tested in the context of fire-modulated wind patterns using high-resolution model simulation. The results show that wind conditions favorable for the initialization of both processes occur, however, with partly substantial differences depending on the environmental preconditions. The direct entrainment of dust particles appears to be an important emission process, particularly under weak wind conditions, while another emission process including larger sand-sized grains becomes more important under strong wind conditions. The unique fire-related aerodynamic preconditions require the development of an adjusted parameterization to describe pyro-convective dust emission together with its influencing factors sufficiently to enable a proper investigation of its atmospheric impacts.

1. Motivation

Vegetation fires have always been an integral component of the Earth system, especially in the semi-arid regions all over the world (e.g., Bowman et al., 2009; Brown et al., 2012; Earl et al., 2015). However, the growing human population in combination with more extensive agricultural activities has shifted the emphasis of fire occurrence from natural wildland fires (e.g., due to lightning strikes) to agriculture-related fires of grass-, crop- and shrublands (e.g., Balch et al., 2017; Liu et al., 2010). Up to date roughly 90% of the global fire activity can be traced back to an anthropogenic origin, predominantly occurring in developing regions such as the Sahel zone (e.g., Andela et al., 2017; Earl et al., 2015). As a further player, the accelerating

climate change has impacted the global fire regime drastically within the most recent past. Changing climate conditions alter the fire risks in many regions around the globe due to shifts in precipitation and temperature patterns. This goes hand in hand with more frequent and intense heat waves eventually leading to temporary or persistent drought conditions (e.g., Bowman et al., 2017; Westerling, 2006). The dried-out vegetation is then more vulnerable to any kind of ignition, which can lead to an increased destructiveness of both natural and prescribed fires. This includes, for example, large parts of Eurasia during the hot and dry spring and summer seasons from 2018 to 2020, the Brazilian rain forests (mainly pushed by arson) in 2019, parts of Australia during the turn of the year 2019/20 (Sanderson & Fisher, 2020) as well as the western US (Higuera & Abatzoglou, 2020). Most of these fires were not just limited to one particular fire type, instead a variety of different landscapes was affected.

In general, the burning vegetation type strongly determines the intensity and destructiveness of a fire as it is usually a function of the available fuel load, that is, the (dry) biomass (e.g., Albini, 1993). While forests can provide a large fuel load and thus are linked to higher burning temperatures, the available fuel load is much more limited in case of grass- and croplands (e.g., Clements et al., 2007). Therefore, these fires are less intense and burn at lower temperatures. This behavior can be expressed by the sensible heat flux generated during the combustion process. Depending on the vegetation type and the environmental conditions, large variations ranging from several $kW\,m^{-2}$ for weak grassland fires to a few thousand $kW\,m^{-2}$ for intense crown fires are observed (Frankman et al., 2013; Lareau & Clements, 2017). Although the heat flux can vary substantially in space and time even within a single fire, a rough categorization can be made: Grassland fires are usually linked to sensible heat fluxes below 100 $kW\,m^{-2}$, while shrubland fires can reach intensities in an order of magnitude of some hundred $kW\,m^{-2}$ (Clements et al., 2007; Frankman et al., 2013; Lareau & Clements, 2017). Stronger heat fluxes are usually linked to natural forest fires, where the major burning center is often elevated from the ground and thus impacts on the soil surface are much more limited (Clark et al., 1999). In contrast, the fire intensity of prescribed forest fires is usually lower and they can burn through the coppice as well and the soil surface may experience stronger impacts.

All kinds of wildland fires are well known as a major hazard due to their huge impacts on the atmosphere, biosphere and society. For instance, they destroy the vegetation cover, threaten the wildlife and the human population; the emitted combustion gases and aerosol particles can harm human health and such fires are found to impact the local weather conditions and even the large-scale climate (e.g., Bowman & Johnston, 2005; Forster et al., 2007; Kumar et al., 2011). While climate effects emerge primarily from the interaction of the fire emissions with the Earth's radiation budget and cloud microphysics, a fire represents also a huge disturbance of the local wind, temperature and stratification patterns. In particular, the fire updraft and the accompanied inflow motions can strongly modulate the wind regime within and around the burning fire area (Clements et al., 2008; Palmer, 1981; Peterson et al., 2015). Furthermore, fires are linked to enduring modifications of the soil surface as the soil characteristics are altered by the fire heat (Dukes et al., 2018; Ravi et al., 2012). A reduction of the soil moisture, modifications of the soil texture as well as changes of the grain size distribution can be observed, which, depending on the fire type, burning temperature, and predominant soil type, result in different impacts on the erodibility of a fire-affected soil surface (Dukes et al., 2018; Kavouras et al., 2012; Pérez-Cabello et al., 2006). This includes both the erosion due to water runoff as well as Aeolian erosion generated by aerodynamic forces. Here, the majority of investigations found an increasing number of fine particles due to breakdown of larger soil aggregates (Albalasmeh et al., 2013; Levin et al., 2012; McNabb & Swanson, 1990), although under some circumstances also the formation of coarse-mode particles can occur as a result of aggregation processes (Blank et al., 1996; Vermeire et al., 2005). As the combustion process also consumes the soil-protecting vegetation cover, the soil surface is at least partly exposed to the atmospheric forces. In concert, both effects lead to a reduction of the required aerodynamic lifting forces for the emission of soil-dust particles as shown by several investigations focusing on post-fire dust emissions (Dukes et al., 2018; Merino-Martín et al., 2014; Ravi et al., 2012; Whicker et al., 2006).

While increased post-fire dust emission fluxes were already the subject of numerous studies (e.g., Dukes et al., 2018; Ravi et al., 2012; Whicker et al., 2006), less attention is paid to the co-emission of soil-dust particles during the fire. However, the interplay of a largely fire-cleared soil surface with the fire's pyro-convective aerodynamic forces does likely enable the emission of soil-dust particles, too. Remote sensing

and in-situ observations have found significant fractions of mineral dust particles within smoke plumes emerging from wildfires in semi-arid regions (Kavouras et al., 2012; Nisantzi et al., 2014; Radke et al., 1991; Schlosser et al., 2017). Despite mixing processes, which may have entrained dust from origins outside the fire, evidence is growing that the strong changes in atmospheric flow patterns within and around a fire are linked directly to the mobilization of soil-dust particles and a subsequent uplift of those particles through the fire's updraft (Kavouras et al., 2012; Palmer, 1981). Particularly, the formation of a convergence close to the surface due to the ascent of heated air can cause a compensating motion that accelerates the horizontal winds and strengthens the near-surface turbulence drastically (Clements et al., 2008; Palmer, 1981). Depending on the fire type and the atmospheric preconditions, these fire-modulated wind forces can be sufficient to mobilize soil particles from the ground, leading to an enrichment of mineral dust particles within the outflow air masses of a fire (Maenhaut et al., 1996; Nisantzi et al., 2014; Radke et al., 1991; Reid et al., 1998).

Such fire-related dust emissions are not yet considered in the classic fire emission modeling, for which so far the main focus lies on the mostly carbonaceous gases and aerosol particles that form as a result of the biomass combustion. However, due to the large fire activity within semi-arid landscapes, fire-induced dust emissions might represent a noteworthy part of the emitted particle mass and thus add to the total atmospheric dust load, especially on a regional scale in the strongest fire-affected areas (Kavouras et al., 2012; Nisantzi et al., 2014; Schlosser et al., 2017). A neglect of this particular dust source could lead to a systematic underrepresentation of the global dust burden and thus to uncertainties concerning the aerosol-climate feedback due to their impacts on the radiation budget or cloud formation (e.g., Tegen & Schepanski, 2018). In addition, if mineral dust is mixed with primary combustion aerosol during the pyro-convectively driven emission process, the physical and chemical properties of the dust particles and eventually their impacts on weather, climate, and human health can be altered (Chalbot et al., 2013; Hand et al., 2010). Thus, a better understanding of the fire-driven dust emission processes is crucial to evaluate these impacts, especially with regard to the anthropogenic interferences that lead to an increase in fire risk in the context of climate change (Jolly et al., 2015; Westerling & Bryant, 2008).

The capability of the enhanced fire-induced winds to mobilize mineral dust particles from the ground was already investigated by Wagner et al. (2018). By defining different fire scenarios, this study has shown that fire can substantially alter the wind patterns in the surrounding area. For instance, the pyro-convective updraft that forms due to the ascent of heated air causes the development of a convergence at the surface, which again leads to an acceleration of the horizontal winds directed toward the convergence zone that is characterized by highly turbulent, convective motions. The main fire updraft and thus the convergence zone forms thereby slightly downwind of the burning fire area if an ambient wind forcing is present such that the enhanced horizontal winds affect particularly the upwind areas. In summary, the study of Wagner et al. (2018) has focused on the changes of the wind speed provoked by the fires and their general ability to exceed typical dust emission threshold velocities rather than on the underlying physical mechanisms leading to those emissions. In contrast, the present study deals with the different emission processes that can take place in the fire environment and investigates the fire-induced changes in the aerodynamic parameters that drive dust emission. We focus on fire setups representative of agricultural grass-, crop- and shrubland fires, where the burning takes place closely above the soil surface and thus fire-related emission of dust particles is more likely. To better understand the potential of pyro-convective aerodynamic forces to emit dust, we apply two conceptually different dust emission parameterizations. Comparison of the dust emissions provides important insights into fire-dust dynamics and serves as a basis to represent fire-related dust emissions on larger spatial scales in the future. The present paper is structured as follows: First, the relevant dust emission mechanisms and their parameterizations are introduced in Section 2. Section 3 focuses on the modeling strategy that is chosen to investigate the research objective outlined above. The corresponding results are presented in Section 4, before a discussion and conclusion closes the paper.

2. Dust Uplift Mechanisms

The wind-driven emission of mineral dust has been a research subject for a long time (Bagnold, 1941; Kok et al., 2012; Shao, 2008). Experimental data and theoretical understanding have revealed that soil particles with a diameter of around 70 μm can be most easily mobilized by the wind drag, as the combined

inter-particle and gravitational forces, that is, the forces that act to keep that particles at the surface, are minimal at this approximate size (Bagnold, 1941; Iversen & White, 1982; Shao & Lu, 2000). The corresponding surface shear stress at which these soil grains get mobilized first is typically expressed as a threshold friction velocity (Shao & Lu, 2000). Once released from the ground and entrained into the air, particles of this size typically perform a hopping motion along the surface (saltation) as they are usually too heavy to stay aloft for long (Bagnold, 1941; Kok et al., 2012; Shao, 2000). At each impact on the ground, smaller dust particles can be released due to inelastic collisions (saltation bombardment) or split-off processes and get entrained into the atmosphere. Due to their smaller weight, the dust particles can remain suspended for longer durations and may enter into a long-range transport mode (Kok et al., 2012; Shao, 2000). Investigations have shown that saltation bombardment (hereafter referred to as SALT) is the most effective dust emission process on a global scale, in particular if strong atmospheric forces are involved (Kok, 2011; Shao et al., 1993). The magnitude of the saltation flux, and hence that of SALT, is driven by the friction velocity u_* (Kok et al., 2014; Lu & Shao, 1999; Marticorena & Bergametti, 1995). In its general form, u_* can be described using the averaged shear stress τ at the surface and the air density ρ_{air}, which again equals to averaged components of the 3D wind u', v', and w' as follows:

$$u_* = \sqrt{\frac{\overline{\tau}}{\rho_{\text{air}}}} = \sqrt{\sqrt{\overline{u'w'}^2 + \overline{v'w'}^2}} \quad . \tag{1}$$

Within the lowermost part of the boundary layer and for neutral atmospheric stratification, u_* can be extracted from the horizontal wind velocity $u(z)$ in the height z as follows:

$$u_* = u(z) \cdot \kappa \cdot \left(\ln\left(\frac{z}{z_0} \right) \right)^{-1} \quad , \tag{2}$$

where κ is the Karman constant of typically 0.4 (Foken, 2006), and z_0 denotes the aerodynamic roughness length. As typical for meso-scale applications, an aerodynamic roughness length of 0.1 m was applied, representative for typical grass- and shrub land dominated landscapes (Foken, 2006). The efficiency at which a soil releases fine dust particles as the result of saltation impacts, that is, the ratio of the dust emission flux to the saltation flux, is called sand-blasting efficiency and depends on the particle size distribution of the present soil (Gillette & Walker, 1977; Kok, 2011; Marticorena & Bergametti, 1995; Shao, 2001).

Smaller dust particles can also be entrained directly into the atmosphere, even under wind conditions that do not exceed the threshold velocities necessary to initiate saltation (Klose et al., 2014; Klose & Shao, 2016; Roney & White, 2004). Even though dust particles are characterized by on average stronger cohesive forces than saltating particles, the direct aerodynamic entrainment of dust particles is facilitated because the strength of the inter-particle cohesive forces can even vary substantially between particles of the same size due to individual particle properties. As a result, aerodynamic forces are able to inject a fraction of the dust particles at the surface directly into the atmosphere (Klose & Shao, 2012; Klose et al., 2014; Zimon, 1982). Under favorable aerodynamic conditions (e.g., within dust devils), the emission strength can be similar or even larger compared to SALT, depending on the availability of loose dust particles (Klose & Shao, 2016; Macpherson et al., 2008; Zhang et al., 2016). Convective-turbulent motions are particularly efficient drivers of aerodynamic entrainment as the large turbulent eddies can transport the necessary momentum down to the surface (Klose & Shao, 2013). The turbulent aerodynamic forces that act on the soil particles can be expressed as an instantaneous momentum flux τ_a. In contrast to the friction velocity u_* that uses the averaged wind properties to calculate dust emission caused by SALT, τ_a takes the current wind components into account. The magnitude of τ_a can be described by

$$\tau_a = \rho_{\text{air}} \sqrt{(u'w')^2 + (v'w')^2} \tag{3}$$

with ρ_{air} as the air density and where u', v', and w' denote the current fluctuations of the 3D mean wind.

3. Methods

Investigations of the dust emission potential provoked by pyro-convection requires detailed knowledge of the aerodynamic conditions within the lowermost levels of the atmosphere. A model with a high spatio-temporal resolution such as large-eddy simulation (LES) can provide the necessary information concerning the fire-modulated near-surface values of the friction velocity u_* and the instantaneous momentum flux τ_a, the

key drivers of dust emission via SALT or CTDE, respectively. The model's complexity was kept simple as the focus lies on the fire impacts on the near-surface wind patterns and the corresponding dust emission potential, without any feedback from the atmosphere on the fire evolution. Thus, we represented the fire by a constant and stationary sensible heat flux at the lower boundary of the model domain as it is typical for agricultural fires burning close to the surface. To ensure realistic ambient atmospheric conditions, the fire was ignited within an already turbulent, well-mixed boundary layer, whose evolution was initiated using a typical atmospheric profile gained from a mesoscale model simulation covering the Sahel zone by Tegen et al. (2013). The study's design is described in further detail in Wagner et al. (2018) where the interested reader can also find a more detailed explanation of the underlying concept of pyro-convectively driven dust emissions. The present investigation builds on that study, however, complemented by further simulations.

In the framework of this study, LES was set up with the All Scale Atmospheric Model (ASAM), a powerful numerical solver that has shown its general suitability over a wide range of atmospheric applications including high resolution small-scale process studies (Doyle et al., 2011; Hinneburg & Knoth, 2005; Jähn et al., 2016). ASAM solves the three-dimensional, fully compressible, non-hydrostatic Euler equations by means of a split-explicit Runge-Kutta time-integration scheme (Jähn et al., 2015; Knoth & Wensch, 2014). The model's architecture allows for a high spatio-temporal resolution at which turbulence can be resolved directly and only a subgrid part needs to be parameterized. The relevant grid spacing close to the surface was set to 10 m, valid for all three dimensions x, y, and z, with an integration time step of 0.2 s and an output time step of 10 s.

In order to capture a wide range of different fire types and atmospheric environments, multiple cases were simulated. Within these simulations either the fire intensity in terms of the fire's sensible heat flux, the actively burning fire size, or the mean geostrophic wind velocity was changed. The fire's sensible heat flux was varied between 50 and 270 $\mathrm{kW\,m^{-2}}$ to capture typical agricultural fire intensities reaching from weak grass- and cropland fires to more intense shrubland fires (e.g., Clements et al., 2007; Frankman et al., 2013; Lareau & Clements, 2017). The reference value of the sensible heat flux for variations of the ambient wind forcing and the burning size was set to 150 $\mathrm{kW\,m^{-2}}$. As the fire intensity can vary widely even within a certain fire type depending on the fuel load, the fire characteristics, and the general environmental conditions, the applied values cannot be linked directly to a specific scenario, however, they lie within a typical range of values representative for the addressed field of application. Variations of the mean geostrophic wind velocity were set to range from quite calm to windier conditions (1–5 $\mathrm{m\,s^{-1}}$) representing characteristic scenarios for low intensity fires burning under largely controlled circumstances. The reference value of 3 $\mathrm{m\,s^{-1}}$, used as background scenario for variations of fire strength and size, has been chosen comparable to wind speeds that are frequently reported by studies focusing on natural fire events or during fire experiments (e.g., Clements et al., 2007; Frankman et al., 2013). Furthermore, the impacts of a changing actively burning fire area on the dust emission potential were considered using size variations reaching from 2,400 to 20,400 $\mathrm{m^2}$. Here, 7,000 $\mathrm{m^2}$ was set as the reference value.

To estimate the vertical dust emission fluxes, we used two fundamentally different parameterizations to gain insight into the potential of fires to emit dust: (a) the parameterization from Marticorena and Bergametti (1995) as refined by Tegen et al. (2002), which represents SALT; and (b) the parameterization from Klose et al. (2014), which represents direct aerodynamic entrainment due to (convective) turbulence (convective turbulent dust emission, CTDE). The chosen SALT parameterization allows for the representation of different soil types expressed by fractions of clay, silt, fine/medium sand, and coarse sand as well as considerations of soil moisture, roughness length and vegetation cover in order to reflect the impacts of surface properties on dust emission. A key part of the SALT parameterization of Marticorena and Bergametti (1995) is the drag partitioning scheme that accounts for roughness elements such as gravels or vegetation. These disturbing elements can consume a part of the momentum provided by the wind that is then not available for dust emission from the soil surface. To express the fraction of the friction velocity u_* that can act on the erodible surface, an effective friction velocity f_{eff} can be used:

$$f_{\text{eff}} = 1 - \left(\frac{\ln\left(\frac{z_0}{z_{0s}}\right)}{\ln\left(0.7\left(\frac{X}{z_{0s}}\right)^{0.8}\right)} \right), \tag{4}$$

with z_{0s} being the smooth roughness length of the soil and z_0 the aerodynamic roughness length associated with the roughness elements (King et al., 2005; Marticorena & Bergametti, 1995; Marticorena et al., 1997). Different estimates have been established for z_{0s} reaching from values defined by the largest grains of the soil ($z_{0s} = D_p$ / 30, e.g., Marticorena and Bergametti (1995)) to significantly larger values in the order of up to 0.1 cm as determined by field studies of bare soil surfaces (Lancaster & Baas, 1998; Wolfe & Nickling, 1996) and suggested by a comparision study of King et al. (2005). The value X can be considered as a measure for the distance how long the flow behind roughness elements is impacted by them and was estimated as $X = 10$ cm by Marticorena and Bergametti (1995). However, based on further measurements, MacKinnon et al. (2004) suggested $X = 12{,}255$ cm to account for non-solid roughness elements such as vegetation and was therefore applied here. In the context of wildfires, this selection may allow for a representation of incompletely burned or unburned vegetation in the fire vicinity. Following the concept of SALT, dust emission (in terms of the vertical dust flux) depends on the friction velocity u_* at the ground. We assumed that the momentum flux is constant within the lowermost levels of the boundary layer and therefore u_* can be extrapolated from the 10 m level. The formulation given by Equation 2 using the logarithmic wind profile assumes neutral atmospheric conditions. In contrast, in the vicinity of fires the lower atmosphere is characterized by heated raising air and thus quite unstable conditions. To take these effects on u_* into account, we applied a stability correction following Benoit (1977) and calculated the friction velocity u_* iteratively based on the lower atmospheric wind and temperature conditions derived from the LES following Equation 6 of Benoit (1977). Furthermore, the parameterization of SALT assumes that saltation is in equilibrium with the atmospheric forcing (Barchyn et al., 2014; Neakrase et al., 2016; Owen, 1964). This premise is more justified for large-scale processes than for small-scale phenomena dominated by turbulence such as the pyro-convectively driven winds. This might lead to a systematic overestimation of the total dust emissions. In the high resolution LES we are using here, u_* represents a grid cell of 10×10 m^2 during 10 s output frequency. We consider this spatio-temporal resolution small enough to represent the characteristics of the pyro-convective flow with a relatively small variability within each grid cell/time step, but large enough to approximately approach a saltation equilibrium within small-scale processes (Neakrase et al., 2016; Spiga et al., 2016). Soil moisture can affect the onset and strength of the emission fluxes by altering the threshold friction velocity. Different concepts exist to account for those impacts. For SALT, we have applied the parameterization based on Fécan et al. (1999) who showed that the threshold friction velocity increases significantly with an increasing soil moisture content as the adsorbtion of water affects the cohesive forces of the soil particles. However, the onset of this increase depends on the soil type and its clay content, and depending on the specific soil, small soil moisture contents do not affect dust emission at all (Fécan et al., 1999).

A parameterization of direct aerodynamic dust entrainment with a special focus on convective-turbulent motions was established by Klose et al. (2014) based on work published in Klose and Shao (2012, 2013). CTDE is described stochastically to take the large variations of the inter-particle cohesive forces and the chaotic nature of the aerodynamic forces within a turbulent atmosphere into account. Hence, probability density functions represent both the soil-dependent cohesive forces and the aerodynamic lifting force as a function of the instantaneous momentum flux τ_a at 10 m height. The CTDE scheme of Klose et al. (2014) also allows for corrections of the dust emission flux for the presence of roughness elements such as vegetation and soil moisture. The soil moisture correction of CTDE considers the effect of soil moisture on the inter-particle cohesive forces, that is, the capillary forces, and the adsorptive film that covers the soil particles (Fécan et al., 1999; McKenna-Neuman & Nickling, 1989), which both ultimately affect the strength of the cohesive forces and thus reduce dust emission strength (Klose et al., 2014). The drag partitioning parameterization from Raupach et al. (1993) was used by Klose et al. (2014) to account for the effect of roughness on the momentum flux. For better comparability with the SALT implementation, we here apply the parameterization of Marticorena and Bergametti (1995) as refined by King et al. (2005) too and express the impacts of roughness elements on the instantaneous momentum flux τ_a instead on the friction velocity as it is done

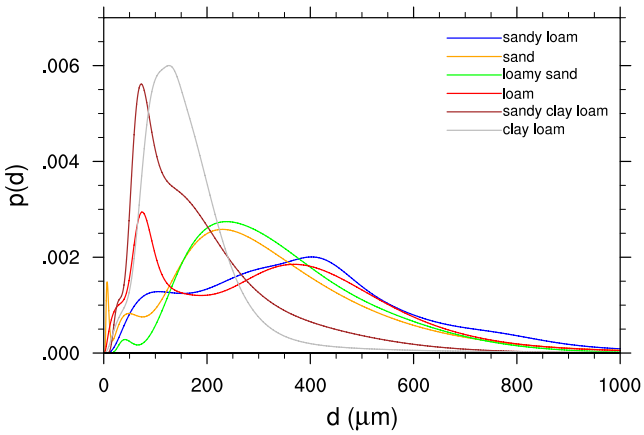

Figure 1. Minimally dispersed particle size distributions of the applied soil types based on the USGS soil texture classes as defined in Klose et al. (2021).

for SALT. The CTDE scheme was calibrated and evaluated against field measurements (Klose et al., 2014) and applied to estimate the dust emission in dust devils (Klose & Shao, 2016). Currently, it only represents the aerodynamic emission of dust particles. The entrainment of larger particles, for example, sand-sized, which could enter into non-equilibrium saltation or even into suspension in strong convective updrafts is not yet included in the scheme. The focus of the parameterization on convective turbulence makes it an excellent test bed to investigate pyro-convectively driven dust emissions through direct aerodynamic entrainment. Both dust emission schemes, the formulation of SALT from Tegen et al. (2002) and the CTDE approach from Klose et al. (2014), were configured with similar but also idealized soil-surface conditions. We have defined a main scenario that is used as a reference with conditions favorable for emission and tested the robustness of this approach by further sensitivity studies. The baseline assumptions for the reference case include a soil moisture of zero, as a consequence of the fire-related dehydration of the soil's top layer due to both the heat impact of the fire and the desiccative effect of the fire winds, and a fully erodible surface. The latter assumes that the fire largely consumed the soil-covering vegetation and left bare soil behind. While that is sufficiently adequate within the actively burning area, in particular for fragile growths such as grass or stubble, it is quite idealized for regions downstream of the fire where the vegetation provides the fuel to keep the fire going, or for shrublands where the hardwood growths are expected to withstand the flames at least partly (Levin et al., 2012) and thus limits the erodible surface. Therefore, we have conducted some sensitivity studies that investigate the impact of an increased surface roughness on the dust emission flux of both schemes. Additional investigations cover the impact of soil moisture on the emission strength for the case that the soil surface may not dry out completely by the fire impact and a residual soil moisture remains. We have used sandy loam as the underlying reference soil type, a very common soil within landscapes affected by agricultural fires such as within the Sahel region (e.g., Chalbot et al., 2013; Dukes et al., 2018; Kavouras et al., 2012). However, agricultural fires are not limited to just one soil type, instead they can also occur in regions where other soil types dominate. Hence, we have also tested other soil types that are present in frequently fire-affected regions. Their particle size distributions were taken from Klose et al. (2021) and are shown in Figure 1. For use with SALT, the particle size distributions have been converted into the four particle size populations used by Tegen et al. (2002) and are given by Table 1. Dust emission caused by SALT requires the so-called sandblasting efficiency α, a measure that transforms the horizontal saltation flux into a vertical dust flux. The sandblasting efficiency was found to be highly dependent on the clay fraction of the soil and can be calculated as follows:

$$\alpha = 10^{(0.134\%_{\text{clay}} - 6)} \tag{5}$$

The resulting values of α for the applied soil types are given in Table 1 as well.

In a nutshell, to investigate fire-related dust emissions, we applied two fundamentally different dust emission approaches, SALT and CTDE, that each rely on different aerodynamic preconditions to generate

Table 1
Corresponding Particle Size Populations of the Applied Soil Types Shown in Figure 1 That are Used for the SALT Scheme Including the Related Value of the Sand Blasting Efficiency α

soil type	$\%_{\text{clay}}$	$\%_{\text{silt}}$	$\%_{\text{medium/fines and}}$	$\%_{\text{coarses and}}$	α (cm)
Sandy loam	0.14	0.2	0.28	0.38	$7.52 \cdot 10^{-5}$
Sand	0.12	0.19	0.28	0.4	$4.06 \cdot 10^{-5}$
Loamy sand	0.01	0.05	0.21	0.73	$1.36 \cdot 10^{-6}$
Loam	0.2	0.23	0.27	0.31	$4.78 \cdot 10^{-4}$
Sandy clay loam	0.04	0.1	0.25	0.61	$3.44 \cdot 10^{-6}$
Clay loam	0.18	0.22	0.27	0.32	$2.58 \cdot 10^{-4}$

particle lifting. The wind regime within the surrounding of agriculture-related fires provides wind conditions that allow for both dust emission processes (Wagner et al., 2018). On the one hand, the near-surface convergence strengthens the inflow winds that are characterized by enhanced friction velocities that enable the initiation of SALT (Clements et al., 2008; Palmer, 1981; Radke et al., 1991; Wagner et al., 2018). On the other hand, the highly turbulent and intense convective updraft motions emerging from fuel consumption create wind gusts, which can directly lift dust particles. To which extent both processes occur in the fire vicinity and how efficiently they can contribute to the total fire-related dust emission is not yet determined. While neither of the schemes is optimized for the fire environment, their application provides insights into the potential dust emission response to the driving aerodynamic forces, the friction velocity u_* and the instantaneous momentum flux τ_a.

4. Results

The fire-induced modulations of the wind field properties and the resulting dust emission fluxes are discussed first in Section 4.1 for the reference case representing a moderate intense shrubfire characterized by a sensible heat flux of 150 $kW\,m^{-2}$ covering an area of 7,000 m^2 and that is exposed to a geostrophic wind forcing of 3 $m\,s^{-1}$, which was initialized in west-east-direction (270°). Subsequently, we analyze the sensitivity of the wind quantities and dust emission fluxes within the actively burning fire area to changes in the ambient wind velocity as well as the impacts of changing fire size and intensity in Section 4.2. These investigations are given with respect to the aerodynamic conditions only, while any soil-surface related properties that can modulate or may even suppress dust emission remain fixed in the first instance. The impacts of changing soil-surface properties such as soil moisture content, surface roughness, and soil type are addressed in Section 4.3.

4.1. General Behavior of Fire-Related Dust Emission Fluxes Due to Wind Field Modulations

Figure 2 provides an overview of the wind field properties and dust emission fluxes obtained for SALT and CTDE. Wagner et al. (2018) have already shown that the near-surface horizontal and vertical wind speeds can be significantly enhanced in the fire environment. Consequently, u_* and τ_a, the quantities that drive dust emission in the SALT and CTDE schemes, are increased with regard to their mean values (Figures 2a and 2b) and even more pronounced with regard to their peak values given as the 90th percentile (Figures 2c and 2d). While Figures 2a and 2c present the fire-impacted properties as spatial contours, Figures 2b and 2d provide horizontal cross-sections orientated in wind direction. Here, the fire-affected values of u_* and τ_a (solid lines) are compared with those under non-fire conditions (dashed lines). Without any fire impacts, the peak values of u_* remain below 0.5 $m\,s^{-1}$. In presence of the fire, the near-surface wind patterns in the surrounding of the active burning become strongly modulated. This results in an increase of the mean friction velocity to values of up to about 0.8 $m\,s^{-1}$ (Figures 2a and 2b) with peaks close to 0.9 $m\,s^{-1}$ (Figures 2c and 2d). The fire impacts on the instantaneous momentum flux τ_a are even more pronounced. Within the non-fire boundary layer, τ_a reaches mean values of 1 $N\,m^{-2}$ and peak values of 2 $N\,m^{-2}$. In contrast, within the fire-modulated atmosphere, τ_a increases at the 10 m level by more than one order of magnitude to mean values around 15 $N\,m^{-2}$ and peak values close to 25 $N\,m^{-2}$, which is certainly sufficient for the initialization of CTDE.

Despite the changes in magnitude of u_* and τ_a, the spatial distributions of the fire-affected quantities reveal noteworthy differences that are visible both in the plan view (Figures 2a and 2c) and the cross sections (Figures 2b and 2d). The friction velocity u_* becomes already enhanced upstream of the actively burning area as a result of the accelerated inflow winds that are directed toward the convergence zone, which has formed in this case due to the impact of the ambient wind at the downstream edge of the fire-heated area and is indicated by the peak values of τ_a. Thus, u_* constantly increases until the convergence point is reached. Downstream, with increasing distance to the active fire, u_* decreases gradually but furthermore remains above-average as the fire-induced momentum is transported by the ambient wind in the present case for roughly another 100 m. This partly results in enhanced horizontal winds there as well. The spatial patterns of the instantaneous momentum flux τ_a behave differently. τ_a becomes slightly enhanced within the actively burning area but does not show significantly increased values upstream of it. However, τ_a suddenly jumps up as the convergence zone comes closer and peaks slightly downstream of the burning area where the

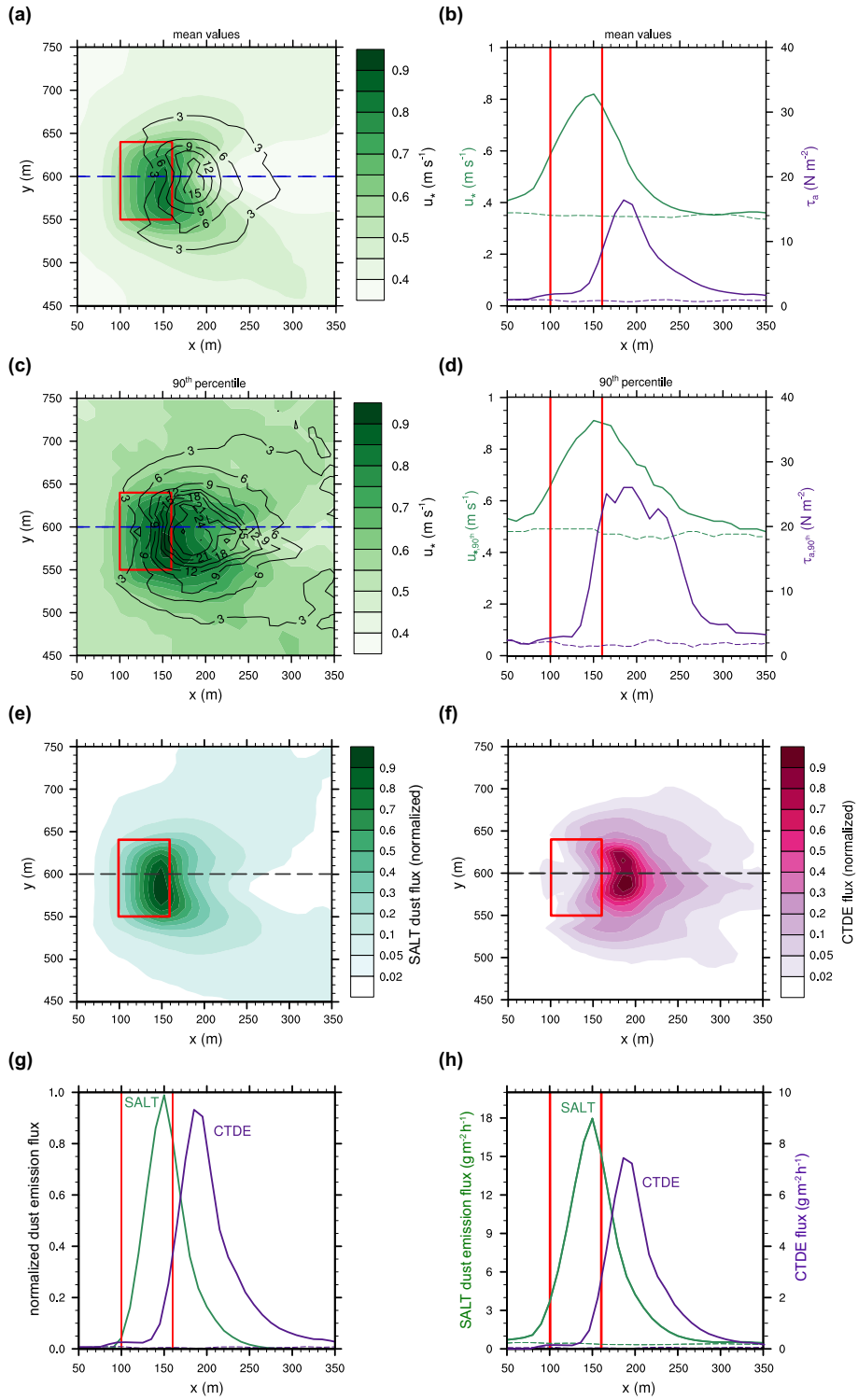

Figure 2.

convergence is located. Here, the main fire updraft has formed and the atmosphere is dominated by the highly convective-turbulent upward motions, which boost τ_a. These turbulence-dominated upwind conditions are also transported downstream so that strongly enhanced τ_a values last for further 100 m before decreasing again quite rapidly toward an average value.

In summary, the wind field quantities the two dust emission parameterizations build on show a quite distinct behavior in the surrounding of the fire. While the friction velocity u_* increases moderately, and this in particular within the actively burning area, the instantaneous momentum flux τ_a is highly sensitive to the fire-induced pyro-convective forces and can increase by more than one order of magnitude. In presence of an ambient wind forcing, this mainly affects the areas downstream of the burning, while the immediate fire area is less affected. Consequently, the application of the corresponding dust emission parameterizations leads to qualitatively and quantitatively different results. Figures 2e and 2f contrast the spatial distribution of the time-averaged dust emission fluxes through SALT (Figure 2e) and of CTDE (Figure 2f). In order to focus on the general characteristics of the emission patterns and taking into account that the underlying soil-surface conditions are highly idealized, the figures represent dust emission fluxes that are normalized by the maximum value of each scheme. Figures 2e and 2f reveal the coincidence of the SALT dust emission fluxes with the areas of the enhanced u_* and that of the CTDE fluxes with increased values of τ_a (cf. Figure 2a). These strong dependencies, which are a direct result from the different parameterizations, determine the relative strength of dust emission with respect to the actively burning fire area. The strongest emissions through SALT occur near the outflow edge of the burning area and largely affect the burning area itself. The strongest CTDE fluxes are located further downstream and occur well outside of the active fire area. This spatial displacement of the peak emission fluxes is particularly visible in the cross-sections shown in Figure 2g. SALT dust emissions peak within the actively burning area, while the peak CTDE fluxes are shifted roughly 50 m downstream. Thus, SALT can be expected to be a more important dust emission process within the burning area as a result of the accelerated inflow winds, while CTDE is more relevant in its outflow edge as there the turbulent-convective updraft motions dominate the wind field. However, the enhanced turbulent motions also lead to slightly enhanced τ_a values within the burning area, which results in small CTDE fluxes upwind and within the first tens of meters into the burning area where the wind field is more dominated by horizontal rather than vertical motions, that reach less than 5% of their maximum strength occurring at the convergence.

In addition to the previous graphs, Figure 2h shows the same situation now using absolute values instead of the normalized values. Due to the idealized character of the underlying soil-surface conditions and the lack of measurement data for evaluation, these values should not be seen already as solid estimates of dust emission fluxes occurring in real fire situations. They rather can provide first insights into which dust emission process might dominate fire-related dust emissions in general, in particular if soil-surface conditions are highly susceptible. The data reveal that the peak dust emissions related to SALT exceed those by CTDE slightly. It is important to note that these estimates do not account for limitations in the availability of either sand particles for saltation or loose dust particles for direct aerodynamic entrainment. So both SALT and CTDE estimates are likely smaller in reality. Although the strength of dust emission via SALT is quite sensitive already to small changes of u_* due to the polynomial proportionality, the highly convective-turbulent environment of the fire-induced wind patterns appears to strongly support CTDE, too. The strength and the extent of the increased values of u_* and τ_a depend of course on the dimension and intensity of the fire as well as on the strength of the ambient geostrophic wind velocity. Therefore, the given values can only be seen as a qualitative picture of how these variables behave in the situation of a fire-modulated wind field.

4.2. Dependency of the Dust Emission Fluxes on Fire Properties and the Ambient Wind Velocity

Figure 3 presents the dependencies of u_* and τ_a as well as the corresponding dust emission fluxes on fire properties such as size and intensity as well as on the ambient wind velocity. The results are shown for the immediate actively burning fire area only, as here the soil-surface conditions are assumingly more suitable

Figure 2. Overview of the fire-affected wind field properties in the 10 m level and the corresponding dust emission fluxes for a simulated fire with a burning size of 7,000 m^2, a sensible heat flux of 150 $kW m^{-2}$, and a geostrophic wind velocity of 3 $m s^{-1}$. Shown are (a) the mean values of the friction velocity u_* (filled contours) and the instantaneous momentum flux τ_a (line contours with a spacing of 3 $N m^{-2}$), (b) a horizontal cross-section of (a) at $y = 600$ m (blue line) comparing the fire-impacted values (solid line) of u_* (green) and τ_a (purple) with those under non-fire conditions (dashed lines), (c) same as (a) but for the 90th percentile, (d) same as (b) but for the 90th percentiles, (e) the normalized dust emission fluxes caused by saltation bombardment (SALT), (f) the normalized convective turbulent dust emission (CTDE) fluxes, (g) horizontal cross-sections of (e) and (f) at $y = 600$ m (black lines) comparing the normalized dust emission fluxes of SALT (green) and CTDE (purple), (h) same as (g) but for the absolute values. The fire area is indicated by a red polygon (a, c, e, and f) or enclosed by red lines (b, d, g, and h). x and y denote the horizontal distance based on the setup of the LES.

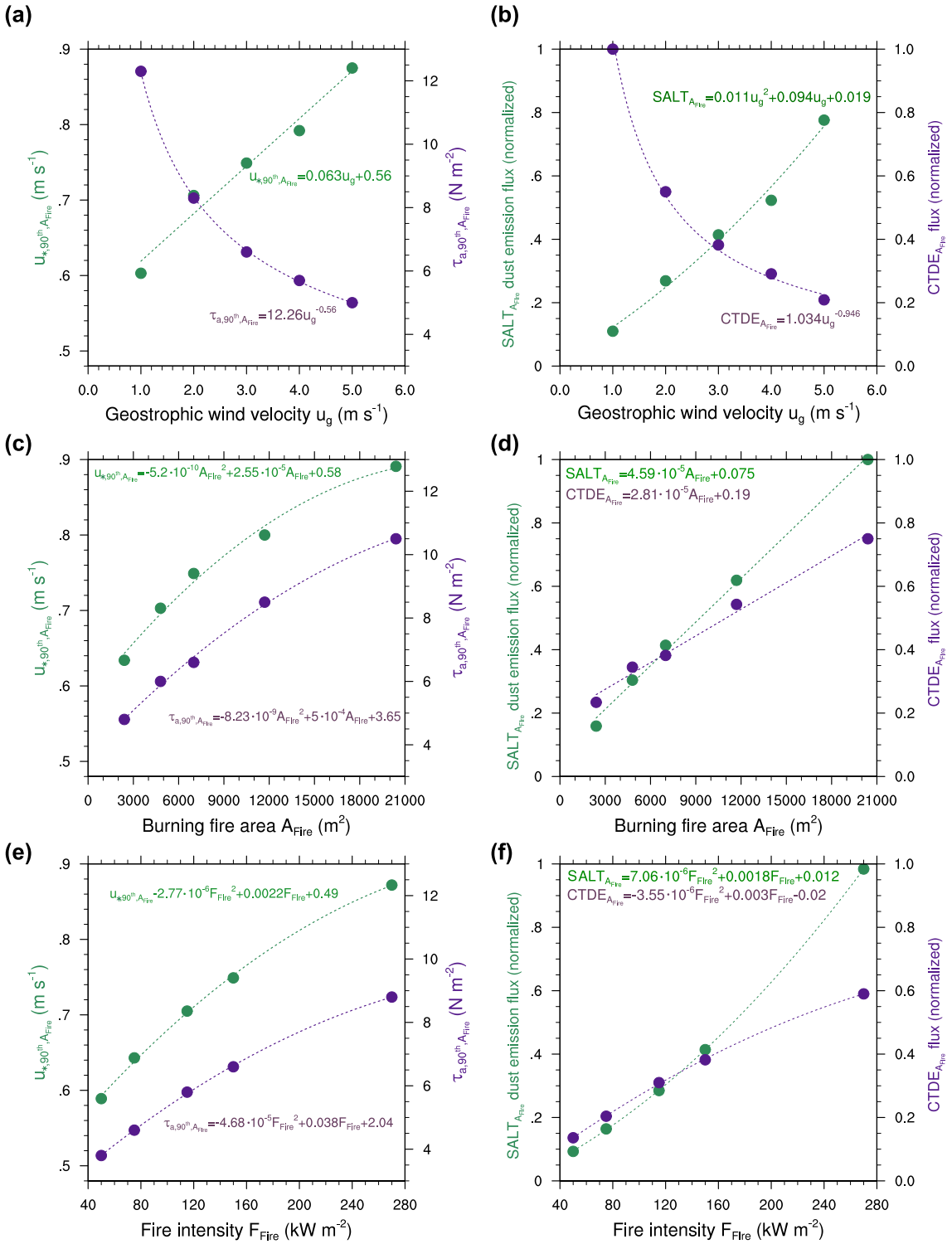

Figure 3. Sensitivity of the key wind field quantities and the corresponding dust emission fluxes to the ambient wind velocity (upper row), the size of the fire area (middle row), and the fire intensity (lower row). Shown are the 90th percentiles of the friction velocity $u_{*,A_{fire}}$ (green) and the instantaneous momentum flux $\tau_{a,A_{fire}}$ (purple) (left column) and the scheme-normalized dust emission fluxes resulting from saltation bombardment (SALT) (green) and convective turbulent dust emission (CTDE) (purple) (right column), each only for the fire area. The resulting regressions of $u_{*,A_{fire}}$, $\tau_{a,A_{fire}}$ and both dust emission fluxes are indicated by the dashed lines. The related regression coefficients are given by Table 2.

Table 2
Coefficients of Determination for the Regressions Shown in Figure 3

parameter	u_*	τ_a	SALT	CTDE
u_g	0.97	1	0.99	0.99
A_{Fire}	0.99	1	1	0.99
F_{Fire}	1	1	1	1

for dust emission than downstream of it and where the application of idealized soil-surface parameters is more justified (cf. Section 3).

Both, the wind field modulations and the dust emissions are positively correlated with the size of the actively burning area and the fire intensity (Figures 3c–3f), while the response to a changing geostrophic wind forcing is more complex (Figures 3a and 3b). First, the fire-impacted friction velocity within the burning area $u_{*,\mathrm{A_{fire}}}$ increases with increasing ambient wind velocity as expected. The fire impact acts as a largely constant offset to the geostrophic wind effect. This results in a rather linear increase of $u_{*,\mathrm{A_{fire}}}$ with the ambient wind (Figure 3a) and based on the general parameterization of SALT in a polynomial growth of the fire-related SALT dust emission flux (Figure 3b). The fire impact on $u_{*,\mathrm{A_{fire}}}$ during weak ambient wind conditions remains relatively small compared to the non-fire values and thus is related to only minor dust emissions. In contrast, large emission fluxes occur for fires exposed to stronger ambient winds. The instantaneous momentum flux τ_a is overall much less susceptible to changes in the ambient wind velocity compared to the fire-related modulations of the wind field. Thus, the fire-driven peak values of τ_a remain in general quite constant (not shown), but if the focus just lies on the actively burning fire area, $\tau_{a,\mathrm{A_{fire}}}$ undergoes a strong decreasing trend with increasing ambient wind velocity (Figure 3a). For the 90th percentile, $\tau_{a,\mathrm{A_{fire}}}$ decreases from 12 $\mathrm{N\,m^{-2}}$ to 5 $\mathrm{N\,m^{-2}}$ as the geostrophic wind increases from 1 to 5 $\mathrm{m\,s^{-1}}$. The pyro-convectively driven CTDE fluxes behave accordingly and reach within the burning fire area only 20% of their strength at an ambient wind speed of 5 $\mathrm{m\,s^{-1}}$ compared to calm conditions with 1 $\mathrm{m\,s^{-1}}$. However, this is still much more than without any fire impact. The at the first glance non-intuitive behavior of decreasing $\tau_{a,\mathrm{A_{fire}}}$ values with increasing ambient wind is caused by the downstream displacement of the main fire updraft when the fire is exposed to stronger ambient wind speeds. As a consequence, the major pyro-convective forces as indicated by τ_a act outside of the actual burning area and thus might limit the potential dust uplift therein (see also Section 4.3). Additionally, the stronger the ambient wind forcing gets, the more the development of the fire updraft is disturbed and the more the fire-generated momentum is transformed into a streamwise motion instead. Both limits the effectiveness of CTDE within the burning fire area despite an increase of the ambient wind speed.

The impacts of changing fire sizes (Figures 3c and 3d) and intensities (Figures 3e and 3f), is such that for the chosen representative fire setups the non-fire values of u_* (0.5 $\mathrm{m\,s^{-1}}$) and τ_a (2 $\mathrm{N\,m^{-2}}$) are always exceeded within the fire area and the typical minimal thresholds to initiate dust emission are reached. However, particularly small and weak fires are related to only small dust emission fluxes through SALT. The relative strength of SALT reaches only up to 5% for the small/weak fires compared to the largest/strongest fire setups. As τ_a reacts much stronger to the fire modulations, already the weakest and smallest fire setups lead to a substantial increase in peak $\tau_{a,\mathrm{A_{fire}}}$ values and thus to noteworthy CTDE fluxes. This applies to both, the relative and the absolute values and highlights again the probably dominant role of CTDE for pyro-convectively driven dust emissions. Interestingly, both of the fire-related peak values of $u_{*,\mathrm{A_{fire}}}$ and $\tau_{a,\mathrm{A_{fire}}}$ react qualitatively quite similar to changes of the fire size and intensity, while the dust emission fluxes diverge more due to the different sensitivities of the parameterizations, which is stronger for SALT to variations of u_* as those of CTDE to changes of τ_a. The application of basic regression methods shows that both the dependency of the peak values of $u_{*,\mathrm{A_{fire}}}$ and $\tau_{a,\mathrm{A_{fire}}}$ as well as the size-normalized dust emission fluxes of the related parameterization approaches on the ambient wind speed and the fire properties can be sufficiently approximated either by linear, polynomial, or reciprocal functions as given by Figure 3.

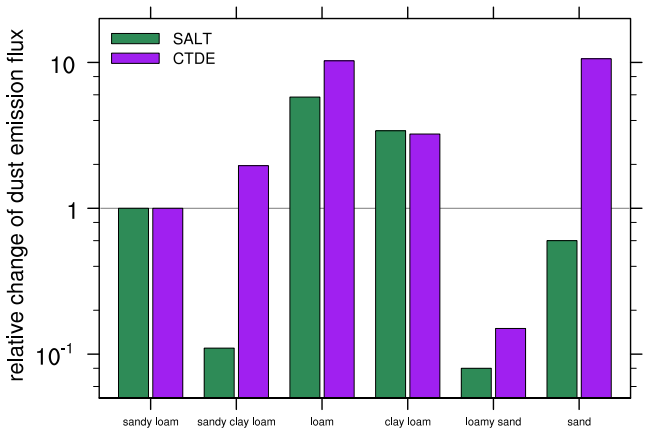

Figure 4. Impact of different soil types on the strength of the fire-related dust emission fluxes of both parameterization schemes. Emission fluxes are normalized to with that of the sandy loam soil and considered for the fire area only.

4.3. Impact of Changing Soil-Surface Conditions on Dust Emission Fluxes

The behavior of the two dust emission schemes was investigated so far only with idealized and homogeneous soil-surface properties such as a soil moisture of zero and a completely fire-cleared surface within and also around the burning fire area. To better understand how a more realistic setup can affect the fire-related dust emission fluxes, further simulations were conducted in which different aerodynamic roughness lengths were assigned for the fire area and its surrounding or where the soil was not completely dry. Furthermore, in addition to the sandy loam soil, we investigated the fire-related dust emission potential of other soil types as shown in Figure 1 or given by Table 1, respectively, which are also common in fire-prone regions. All additional simulations are compared to our idealized reference scenario that was discussed in detail in Section 4.1. Therefore, the fire-related dust emission fluxes within this section are always normalized to those of the reference simulation.

Figure 4 shows the dust emission fluxes obtained for different soil types. It can be seen that normalized fire-related dust emission fluxes vary by almost two orders of magnitude across the different soil types. For individual soil types, SALT and CTDE differ in behavior, too. The changes in the SALT dust fluxes are largely caused by the different values of the sandblasting efficiency and result in comparably small dust emission fluxes for the sandy clay loam and loamy sand soil due to their small clay content, while loam and clay loam emit more dust compared to our reference of sandy loam soil. For most of the soil types, the fire-related CTDE fluxes behave similar to those of SALT, however, the sandy clay loam and sand soils stand out as their effects are opposite in the SALT and CTDE results. Our results demonstrate that the fire-related dust emissions are sensitive to soil texture in both the SALT and CTDE scheme and that sandy loam, our reference soil type, seems to be intermediate in emissivity for both mechanisms. If a soil with a large fraction of sand-sized particles is additionally characterized by a topsoil layer composed of fine dust particles (e.g., the applied sand soil), SALT can become an even more effective dust generation process after the fine topsoil material is exhausted by CTDE. The sometimes strong fire-related updrafts may be able to emit also particles larger than 20 m. This cannot be tested in our current setup, but it would increase the dust emission fluxes for soil types with a larger coarse dust and sand fraction. Furthermore, the strong surface heating caused by the fire can modify the soil's particle size distributions as larger particles may disintegrate or oppositely form due to aggregation processes (e.g., Levin et al., 2012; McNabb & Swanson, 1990; Vermeire et al., 2005). This would also affect the inter-particle binding forces of the dust particles and thus the erodibility of the soil but the implications of these complex interactions cannot be addressed in the framework of this study.

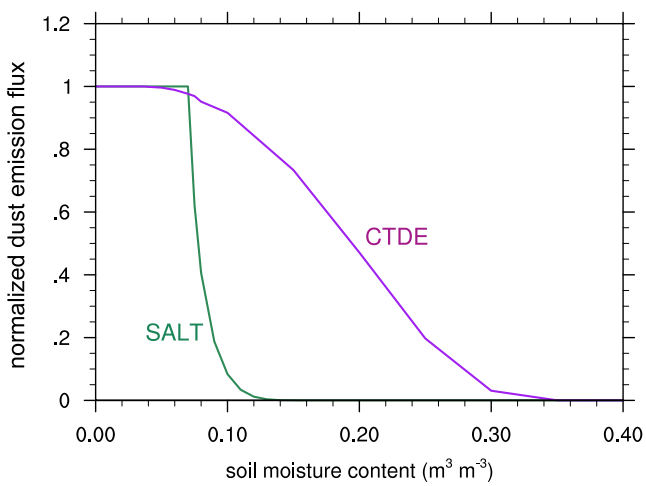

Figure 5. Dependency of the fire-related dust emission fluxes within the fire area on the soil moisture content for convective turbulent dust emission (CTDE) (purple) and saltation bombardment (SALT) (green). The emission strength is normalized for each scheme.

The dependency of the normalized fire-related dust emission fluxes within the fire area on the soil moisture content is given by Figure 5. Small soil moisture contents do not impact dust emission fluxes as the adsorption of small amounts of water does not significantly alter the cohesive forces of the soil particles and thus dust emission is not affected (e.g., Fécan et al., 1999). When the soil moisture increases further, the dust emission fluxes decrease. In the case of SALT, soil moisture is accounted for in terms of an increased threshold friction velocity for the initialization of SALT, which starts to be effective at values of 0.07 $m^3 m^{-3}$. The reduction of dust emission occurs quite rapidly and already at a soil moisture content of around 0.1 $m^3 m^{-3}$ the dust emission fluxes caused by SALT become largely negligible. In contrast, the reduction of the CTDE fluxes, whose parameterization does not consider the threshold friction velocity but quantifies the effect of an increasing soil moisture content on the cohesive/capillary forces, occurs much more gradually and emissions

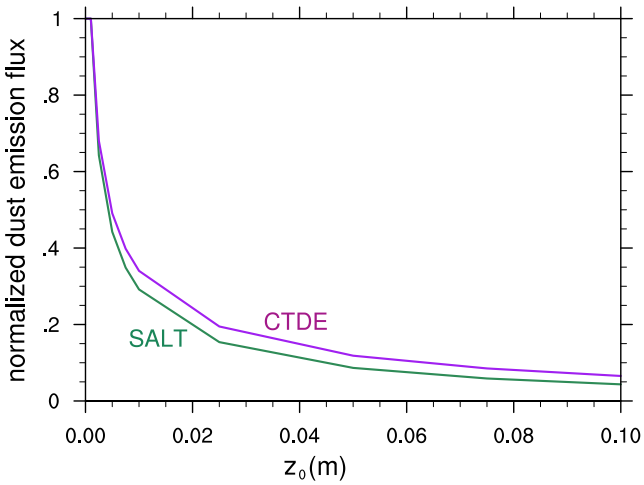

Figure 6. Dependency of the normalized fire-related dust emission fluxes on the aerodynamic roughness length z_0.

remain noteworthy up to soil moisture contents of close to $0.3\,m^3m^{-3}$. Hence, even relatively wet soil surfaces would not completely impede fire-related dust emissions based on the tested parameterizations and parameters, in particular CTDE. In general, the combination of the fire heat and the increased evaporation caused by the strong (and hot) fire-related winds leads to a quick drying of the uppermost soil layer (Gillette, 1999; Tegen et al., 2002) and can easily reduce the soil moisture content to values close to zero. The assumption of a largely dry soil therefore appears plausible.

The presence of roughness elements can have huge impacts on the strength of dust emission fluxes. In the context of agricultural fires, such roughness elements might be vegetation remnants such as hardwood growths that survive the fire impact within the burning area or that have simply not yet been affected by the fire. The effect of roughness elements on dust emission is twofold: First, they cover a part of the soil surface preventing dust emission. Second, they consume a part of the momentum provided by the wind that is then not available for the mobilization of the soil grains. While the cover fraction reduces the erodible area in its simplest form linearly, the effect of drag partitioning is more complex. Here we use the drag partitioning parameterization of Marticorena and Bergametti (1995) as given by Equation 4 for both SALT (applied to the friction velocity u_*) and CTDE (applied to the instantaneous momentum flux τ_a). It depends mainly on the aerodynamic roughness length z_0, which again is determined by the presence of vegetation and their height and spacing. The larger z_0, the more momentum provided by the aerodynamic forces is consumed by the roughness elements and consequently not available for dust emission. Figure 6 shows the dependency of the normalized dust emission fluxes on z_0. Dust emissions are strongly reduced with increasing roughness and the reduction occurs qualitatively similar for both dust emission schemes. To mimic a fire scenario in which vegetation is consumed within the fire area, but present around it, we apply different values for z_0. Figure 7 shows the resulting normalized dust emission fluxes for different reductions of z_0 within the fire area that vary between 0.5 and 2 orders of magnitude. As expected, the fire area becomes now much more dominant for dust emission, while the regions downstream contribute less to the total dust emissions. This effect does not affect SALT too strongly as here the main dust emission occurs within the fire area anyway. In contrast, the overall contribution of CTDE gets significantly reduced, at least in the cases with a significant ambient wind forcing as here the peak CTDE fluxes are found largely downwind of the fire area. However, as long as the roughness outside of the fire area becomes not too large, CTDE is fostered there nonetheless, although overall weakened. We note that the quantitative reduction of both SALT and CTDE with increasing surface roughness is sensitive to the parameterization used (e.g., Marticorena & Bergametti, 1995; Raupach et al., 1993) and to the parameters therein, such as X in the case of the Marticorena and Bergametti (1995) parameterization (see Section 3).

5. Discussion and Conclusion

We applied two fundamentally different dust emission parameterizations - one representing saltation-generated dust emission (SALT) driven by the friction velocity u_*, and the other one describing direct aerodynamic dust entrainment by convective turbulence (CTDE) governed by the instantaneous momentum flux τ_a - to investigate the dust emission potential of agricultural fires based on LES fire-modulated atmospheres. Both u_* and τ_a are strongly modified by pyro-convection. Our analyses have shown that aerodynamic conditions favorable for the initialization of SALT and CTDE exist in nearly all of the investigated fire setups representative for typical agriculture-related burning conditions. Both dust emission parameterization schemes produced considerable amounts of mineral dust in the vicinity of the burning area. However, important differences exist between the resulting SALT and CTDE fluxes within and outside of the burning area, for example, if the atmospheric wind forcing or the fire characteristics such as intensity or the size of the burning area change. These differences are caused by the fire-modulated near-surface aerodynamic situation, which is characterized by two dominant wind regimes. Close to the convergence zone, usually

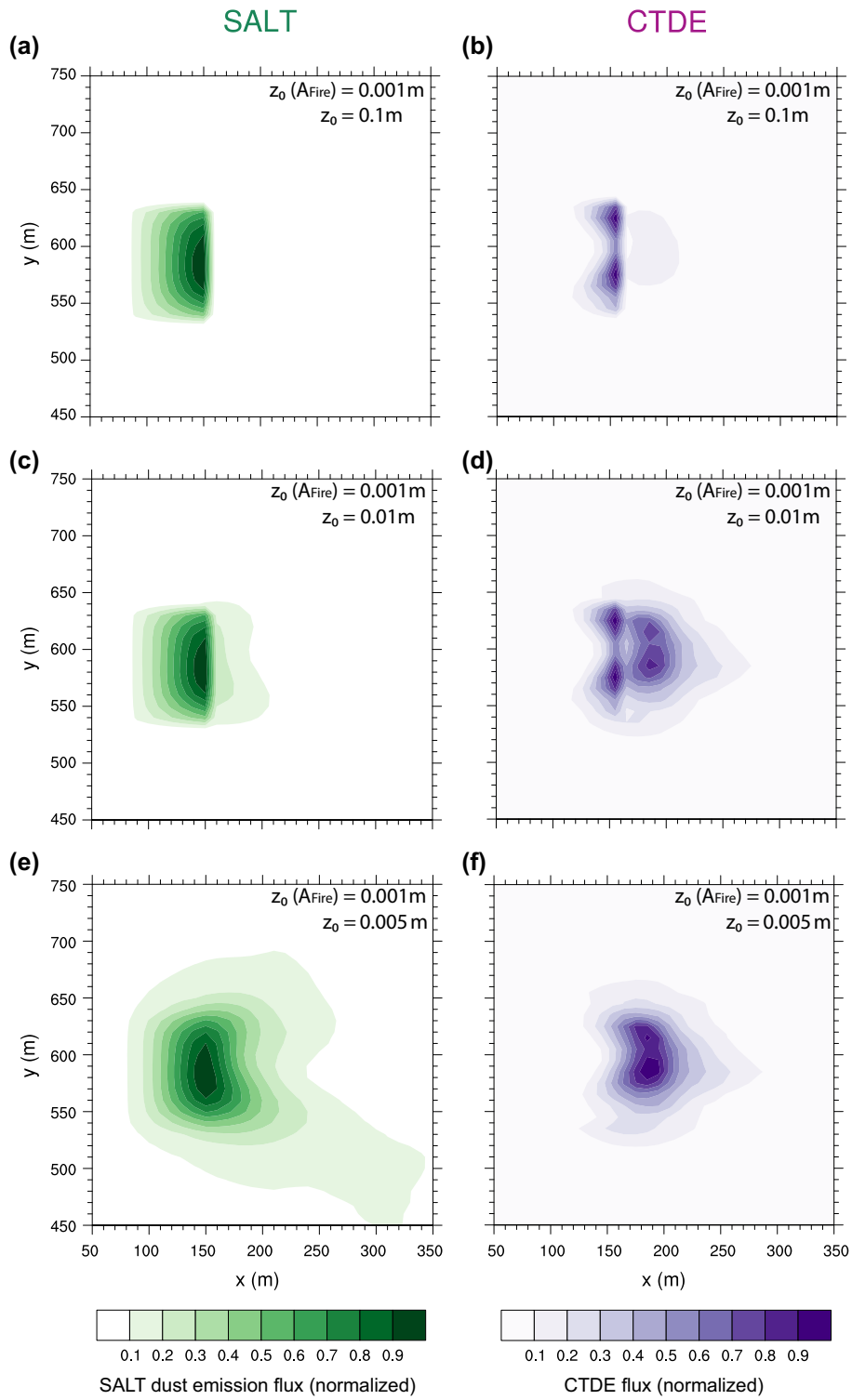

Figure 7. Variation of the normalized dust emission fluxes of saltation bombardment (SALT) and convective turbulent dust emission (CTDE) if the aerodynamic roughness length z_0 within the fire area is different (lower) compared to its surrounding. Specific values for z_0 are given in the panels.

at the downward end of the fire area, the atmosphere is dominated by convective-turbulent upward motions, favoring CTDE. Upstream of the convergence zone, mostly within the burning area, the accelerated horizontal winds blowing toward the convergence area are characterized by increased friction velocities that ultimately promote SALT. Of course, both wind regimes superimpose to some degree and are strongly controlled by the ambient wind forcing. Therefore, in particular within the actively burning fire area, the aerodynamic conditions are favorable for dust emissions due to both processes, however, with different intensities depending on the exact location and the fire and environmental wind conditions.

The scheme-normalized dust emission fluxes within the immediate burning fire area were found to be strongly dependent on variations of basic fire and wind field parameters. This provides useful starting points for further investigations, as the impact of the ambient wind velocity, the size of the burning fire area and the fire intensity on dust emission can be approximated for both dust emission processes by simple regression types. The parameters needed for a future implementation of pyro-convectively driven dust emission into aerosol-atmosphere models can be retrieved either from satellite observations monitoring the wildfire activity or are available from the model meteorology. While increasing fire intensities and larger burning areas generally lead to stronger dust emission fluxes independent of the dust emission process, the opposing impact of changing ambient wind speeds may have noticeable implications for real fires. Within the burning area, the strength of SALT decreases if the ambient wind becomes less intense, while CTDE increases. This is due to the fire updraft, which is located above the fire in weak-wind conditions, and which leads only to comparably small increases of $u_{*,\mathrm{A_{fire}}}$ (relevant for SALT), but to strong increases of $\tau_{a,\mathrm{A_{fire}}}$ (relevant for CTDE). Consequently, a parameterization representing SALT does not produce significantly enhanced dust emissions in such weak-wind cases. However, taking the current formulation of CTDE as a baseline implies that even weak agricultural management fires, which are preferably ignited during low-wind conditions, can be linked to an injection of a considerable amount of mineral dust into the atmosphere. If this can be proven correct by further investigations, the potential of such prescribed agricultural fires as source of mineral dust emission might be substantial and can have a considerable atmospheric relevance. For agricultural fires, CTDE can be a very important dust emission process due to the pyro-convective forces inducing strong modulations to the instantaneous momentum flux . Even though the friction velocity is less strongly affected, during favorable conditions (i.e., particularly strong burns or fires with a strong background wind forcing) the contribution of SALT generated by gusts can be significant and may even dominate over CTDE. Therefore, both processes are important if fire-induced dust emissions are described.

So far, our study's design is idealized and the dust emission schemes are not yet adjusted to natural fire conditions, first and foremost with respect to the soil-surface conditions. These simplifications include an unlimited particle supply from a completely dry sandy loam soil surface whose properties were not altered by fire impacts. Furthermore, we assumed a complete removal of the vegetation cover within the burning area as a result of the combustion process. This may be sufficiently fulfilled for crops and grasslands, but remains highly idealized for shrubs. Here, the unburned vegetation remnants would act as further roughness elements within the flow and consume a larger part of the momentum provided by the pyro-convective forces that is then not available for dust mobilization. Sensitivity studies have shown that increasing roughness and a larger soil moisture content reduce dust emission for both processes, however, under conditions typical for a burning fire, this reduction should not prevent dust emission at all. On the other hand, in particular during situations where the aerodynamic forcing is already weak, even a comparably small increase of the surface roughness (e.g., due to vegetation debris or larger ash particles) might suppress dust emission more effectively.

Although the strongest emission fluxes are found within or close to the actively burning area as here the heat release of the fire has the strongest impacts on the aerodynamic conditions, the fire-generated turbulence can be transported further downstream by the ambient wind into a larger surrounding of the burning activity. While within the actively burning area, soil-surface conditions more susceptible to wind erosion can be assumed, the situation is different for the surrounding areas. However, if patches of bare soil are present, which is typical in many semi-arid landscapes such as these dominated by heterogeneously distributed shrubs (Dukes et al., 2018), dust emission can be generated here as well. Such situations would again facilitate CTDE as the interaction of the fire-related wind flow with the vegetation can increase the turbulence locally (Klose et al., 2014) and CTDE may still be an effective emission process under such conditions.

However, this is highly case-dependent and cannot be generalized although a probabilistic approach seems feasible. Nevertheless, according to the generally more appropriate soil-surface conditions within the burning fire area, the main focus for further developments should lay here initially.

An explicit representation of pyro-convectively driven dust emissions in large-scale aerosol-atmosphere models is necessary to quantify the regional and global relevance of this emission pathway, in particular with respect to other emission processes. Therefore, a parameterization approach is required that accounts for both dust emission processes and prioritizes their contribution depending on the specific fire and environmental conditions. It should also include the impacts of an incomplete vegetation combustion depending on the particular fire type and account for fire-specific soil properties. The latter might include, if available, locally modified particle size distributions typical for a fire-altered soil type and possible effects of the fire on soil-surface cohesion, which would affect both dust emission processes. While post-fire soil properties are known, the exact soil conditions during a fire remain a source of uncertainty. All those limitations make it difficult to really quantify the importance of this specific emission process yet. However, using the results of the current study, it is already feasible to derive a first rough estimate of the contribution of fire-related dust emissions on a global scale. Based on the strength of the simulated dust emission fluxes within the fire area and taking their variability resulting from different wind velocities and fire properties into account, they can provide a starting point and be scaled up by using data of the global burned area. The mean dust emission fluxes within the fire area lie in the order of roughly 1–20 $g\,m^{-2}h^{-1}$ depending on the scenario, whereby all possible emissions in the vicinity of the immediate fire area are ignored for simplification. The average global burned area accounts for 404 $Mha\,yr^{-1}$, of which 57% are shrub-, grass-, croplands, and savannas (Randerson et al., 2012). Under the assumption of a burning duration of 1 h, this scales up to fire-related dust emission fluxes of roughly 2–45 $Tg\,yr^{-1}$. Taking recent model estimates as a baseline, which determined the global dust emission in the size range of 0.06–20 μm to 735–3,598 $Tg\,yr^{-1}$ (Wu et al., 2020), would mean that such fires might contribute 0.06%–6% to the global dust emissions. Such fire-related dust emissions appear particularly relevant as they would largely occur outside of typical dust emitting regions such as the global dust belt. However, the limitations of our simulations mentioned above lead to a large range of uncertainty. This includes several aspects such as the emission of larger and heavier particles in stronger fires, or dust emissions in the surrounding of the burning area, but also a severe reduction of the dust emission fluxes due to a remaining soil coverage or further fire impacts on the soil properties. To reduce uncertainty, it is important that in addition to a further optimization of the dust emission parameterization also more detailed measurements and field studies are conducted that address dust emission in the context of fires and their concomitants, which would help to prove/manifest or to revise the findings of this idealized model study. Eventually, such a dust emission parameterization tuned for fire conditions enables us to determine the amount of mineral dust that is emitted through pyro-convection. This appears especially relevant as many kinds of environmental fires are supposed to increase in number, frequency, and intensity as a response to climate change (Bowman et al., 2017; Jolly et al., 2015; Westerling & Bryant, 2008). If the related fraction of fire-induced dust emissions can be estimated properly, the climate impacts of airborne mineral dust in general and that of dust mixed with combustion aerosol as a consequence of the fire-emission can be evaluated more precisely.

Data Availability Statement

The data used for the analysis are available at Zenodo, see Wagner (2021).

Acknowledgments
R. Wagner and K. Schepanski thank the German Research Foundation (Deutsche Forschungsgemeinschaft, DFG) for funding the project SCHE 1678/5–1. M. Klose has received funding from the European Union's Horizon 2020 research and innovation program under the Marie Skłodowska-Curie grant agreement No. 789630 and from the Helmholtz Association's Initiative and Networking Fund (grant agreement no. VH-NG-1533). The authors acknowledge the Center for Information Services and High performance Computing (ZIH) of the Technische Universität Dresden (TU Dresden) for providing computing capacity. The authors are grateful to the three anonymous reviewers for their valuable comments and suggestions that helped to improved the quality of the paper. Open access funding enabled and organized by Projekt DEAL.

References

Albalasmeh, A. A., Berli, M., Shafer, D. S., & Ghezzehei, T. A. (2013). Degradation of moist soil aggregates by rapid temperature rise under low intensity fire. *Plant and Soil*, *362*(1–2), 335–344. https://doi.org/10.1007/s11104-012-1408-z

Albini, F. (1993). Dynamics and Modeling of Vegetation Fires: Observations. In P. J. Crutzen, & J. G. Goldammer (Eds.), *Fire in the environment: The ecological, atmospheric, and climatic importance of vegetation fires* (pp. 39–52). John Wiley & Sons Inc.

Andela, N., Morton, D., Giglio, L., Chen, Y., van der Werf, G., Kasibhatla, P., et al. (2017). A human-driven decline in global burned area. *Science*, *356*(6345), 1356–1362. https://doi.org/10.1126/science.aal4108

Bagnold, R. A. (1941). *The physics of blown sand and Desert Dunes*: Methuen.

Balch, J. K., Bradley, B. A., Abatzoglou, J. T., Nagy, R. C., Fusco, E. J., & Mahood, A. L. (2017). Human-started wildfires expand the fire niche across the United States. *Proceedings of the National Academy of Sciences*, *114*(11), 2946–2951. https://doi.org/10.1073/pnas.1617394114

Barchyn, T. E., Martin, R. L., Kok, J. F., & Hugenholtz, C. H. (2014). Fundamental mismatches between measurements and models in aeolian sediment transport prediction: The role of small-scale variability. *Aeolian Research*, *15*, 245–251. https://doi.org/10.1016/j.aeolia.2014.07.002

Benoit, R. (1977). On the integral of the surface layer profile-gradient functions. *Journal of Applied Meteorology*, *16*(8), 859–860. https://doi.org/10.1175/1520-0450(1977)016<0859:OTIOTS>2.0.CO;2

Blank, R. R., Allen, F. L., & Young, J. A. (1996). Influence of simulated burning of soil-litter from Low Sagebrush, Squirreltail, Cheatgrass, and Medusahead on water-soluble anions and cations. *International Journal of Wildland Fire*, *6*(3), 137–143. https://doi.org/10.1071/WF9960137

Bowman, D. M., Balch, J. K., Artaxo, P., Bond, W. J., Carlson, J. M., Cochrane, M. A., et al. (2009). Fire in the earth system. *Science*, *324*(5926), 481–484. https://doi.org/10.1126/science.1163886

Bowman, D. M., & Johnston, F. H. (2005). Wildfire smoke, fire management, and human health. *EcoHealth*, *2*(1), 76–80. https://doi.org/10.1007/s10393-004-0149-8

Bowman, D. M., Williamson, G. J., Abatzoglou, J. T., Kolden, C. A., Cochrane, M. A., & Smith, A. M. (2017). Human exposure and sensitivity to globally extreme wildfire events. *Nature Ecology & Evolution*, *1*(3), 0058. https://doi.org/10.1038/s41559-016-0058

Brown, S. A., Scott, A. C., Glasspool, I. J., & Collinson, M. E. (2012). Cretaceous wildfires and their impact on the Earth system. *Cretaceous Research*, *36*, 162–190. https://doi.org/10.1016/j.cretres.2012.02.008

Chalbot, M.-C., Nikolich, G., Etyemezian, V., Dubois, D., King, J., Shafer, D., et al. (2013). Soil humic-like organic compounds in prescribed fire emissions using nuclear magnetic resonance spectroscopy. *Environmental Pollution*, *181*, 167–171. https://doi.org/10.1016/j.envpol.2013.06.008

Clark, T. L., Radke, L., Coen, J., & Middleton, D. (1999). Analysis of small-scale convective dynamics in a crown fire using infrared video camera imagery. *Journal of Applied Meteorology*, *38*(10), 1401–1420. https://doi.org/10.1175/1520-0450(1999)038<1401:AOSSCD>2.0.CO;2

Clements, C. B., Zhong, S., Bian, X., Heilman, W. E., & Byun, D. W. (2008). First observations of turbulence generated by grass fires. *Journal of Geophysical Research*, *113*(D22), D22102. https://doi.org/10.1029/2008JD010014

Clements, C. B., Zhong, S., Goodrick, S., Li, J., Potter, B. E., Bian, X., et al. (2007). Observing the dynamics of wildland grass fires: FireFlux – A field validation experiment. *Bulletin of the American Meteorological Society*, *88*(9), 1369–1382. https://doi.org/10.1175/BAMS-88-9-1369

Doyle, J. D., Gaberšek, S., Jiang, Q., Bernardet, L., Brown, J. M., Dörnbrack, A., et al. (2011). An intercomparison of T-REX mountain-wave simulations and implications for mesoscale predictability. *Monthly Weather Review*, *139*(9), 2811–2831. https://doi.org/10.1175/MWR-D-10-05042.1

Dukes, D., Gonzales, H. B., Ravi, S., Grandstaff, D. E., Van Pelt, R. S., Li, J., et al. (2018). Quantifying postfire Aeolian sediment transport using rare earth element tracers. *Journal of Geophysical Research: Biogeosciences*, *123*(1), 288–299. https://doi.org/10.1002/2017JG004284

Earl, N., Simmonds, I., & Tapper, N. (2015). Weekly cycles of global fires – Associations with religion, wealth and culture, and insights into anthropogenic influences on global climate. *Geophysical Research Letters*, *42*(21), 9579–9589. https://doi.org/10.1002/2015GL066383

Fécan, F., Marticorena, B., & Bergametti, G. (1999). Parameterization of the increase of the aeolian erosion threshold wind friction velocity due to soil moisture for arid and semi-arid areas. *Annales Geophysicae*, *17*, 149–157. https://doi.org/10.1007/s00585-999-0149-7

Foken, T. (2006). *Angewandte meteorologie*. Springer Berlin Heidelberg. https://doi.org/10.1007/978-3-540-38204-1

Forster, P., Ramaswamy, V., Artaxo, P., Berntsen, T., Betts, R., Fahey, D. W., & Miller, H. (2007). Changes in Atmospheric Constituents and in Radiative Forcing. In D. Q. M. M. Z. C. M. M. K. A. M. T. S. Solomon, & H. Miller (Eds.), *Climate change 2007: The physical science basis. contribution of working group i to the fourth assessment report of the intergovernmental panel on climate change*: Cambridge University Press.

Frankman, D., Webb, B. W., Butler, B. W., Jimenez, D., Forthofer, J. M., Sopko, P., et al. (2013). Measurements of convective and radiative heating in wildland fires. *International Journal of Wildland Fire*, *22*(2), 157–167. https://doi.org/10.1071/WF11097

Gillette, D. (1999). A qualitative geophysical explanation for "hot spot" dust emitting source regions. *Contributions to Atmospheric Physics*, *72*.

Gillette, D., & Walker, T. R. (1977). Characteristics of airborne particles produced by wind erosion of sandy soil, high plains of west Texas. *Soil Science*, *123*(2), 97–110. https://doi.org/10.1097/00010694-197702000-00004

Hand, V. L., Capes, G., Vaughan, D. J., Formenti, P., Haywood, J. M., & Coe, H. (2010). Evidence of internal mixing of African dust and biomass burning particles by individual particle analysis using electron beam techniques. *Journal of Geophysical Research*, *115*(D13), D13301. https://doi.org/10.1029/2009JD012938

Higuera, P. E., & Abatzoglou, J. T. (2020). Record-setting climate enabled the extraordinary 2020 fire season in the western United States. *Global Change Biology*. https://doi.org/10.1111/gcb.15388

Hinneburg, D., & Knoth, O. (2005). Non-dissipative cloud transport in Eulerian grid models by the volume-of-fluid (VOF) method. *Atmospheric Environment*, *39*(23), 4321–4330. https://doi.org/10.1016/j.atmosenv.2005.02.027

Iversen, J. D., & White, B. R. (1982). Saltation threshold on Earth, Mars and Venus. *Sedimentology*, *29*, 111–119. https://doi.org/10.1111/j.1365-3091.1982.tb01713.x

Jähn, M., Knoth, O., König, M., & Vogelsberg, U. (2015). ASAM v2.7: A compressible atmospheric model with a Cartesian cut cell approach. *Geoscientific Model Development*, *8*(2), 317–340. https://doi.org/10.5194/gmd-8-317-2015

Jähn, M., Muñoz-Esparza, D., Chouza, F., Reitebuch, O., Knoth, O., Haarig, M., & Ansmann, A. (2016). Investigations of boundary layer structure, cloud characteristics and vertical mixing of aerosols at Barbados with large eddy simulations. *Atmospheric Chemistry and Physics*, *16*(2), 651–674. https://doi.org/10.5194/acp-16-651-20110.5194/acp-16-651-2016

Jolly, W. M., Cochrane, M. A., Freeborn, P. H., Holden, Z. A., Brown, T. J., Williamson, G. J., & Bowman, D. M. (2015). Climate-induced variations in global wildfire danger from 1979 to 2013. *Nature Communications*, *6*, 7537. https://doi.org/10.1038/ncomms8537

Kavouras, I. G., Nikolich, G., Etyemezian, V., DuBois, D. W., King, J., & Shafer, D. (2012). In situ observations of soil minerals and organic matter in the early phases of prescribed fires. *Journal of Geophysical Research*, *117*(D12), D12313. https://doi.org/10.1029/2011JD017420

King, J., Nickling, W. G., & Gillies, J. A. (2005). Representation of vegetation and other nonerodible elements in aeolian shear stress partitioning models for predicting transport threshold. *Journal of Geophysical Research*, *110*(F4). https://doi.org/10.1029/2004JF000281

Klose, M., Jorba, O., Gonçalves Ageitos, M., Escribano, J., Dawson, M. L., Obiso, V., et al. (2021). Mineral dust cycle in the Multiscale Online Nonhydrostatic AtmospheRe CHemistry model (MONARCH) Version 2.0. *Geoscientific Model Development Discussions*, 1–59. https://doi.org/10.5194/gmd-2021-32.2021

Klose, M., & Shao, Y. (2012). Stochastic parameterization of dust emission and application to convective atmospheric conditions. *Atmospheric Chemistry and Physics*, *12*(16), 7309–7320. https://doi.org/10.5194/acp-12-7309-2012

Klose, M., & Shao, Y. (2013). Large-eddy simulation of turbulent dust emission. *Aeolian Research*, *8*, 49–58. https://doi.org/10.1016/j.aeolia.2012.10.010

Klose, M., & Shao, Y. (2016). A numerical study on dust devils with implications to global dust budget estimates. *Aeolian Research*, *22*, 47–58. https://doi.org/10.1016/j.aeolia.2016.05.003

Klose, M., Shao, Y., Li, X., Zhang, H., Ishizuka, M., Mikami, M., & Leys, J. F. (2014). Further development of a parameterization for convective turbulent dust emission and evaluation based on field observations. *Journal of Geophysical Research: Atmosphere*, *119*(17), 10441–10457. https://doi.org/10.1002/2014JD021688

Knoth, O., & Wensch, J. (2014). Generalized split-explicit Runge–Kutta methods for the compressible Euler equations. *Monthly Weather Review*, *142*(5), 2067–2081. https://doi.org/10.1175/MWR-D-13-00068.1

Kok, J. F. (2011). Does the size distribution of mineral dust aerosols depend on the wind speed at emission? *Atmospheric Chemistry and Physics*, *11*(19), 10149–10156. https://doi.org/10.5194/acp-11-10149-2011

Kok, J. F., Mahowald, N. M., Fratini, G., Gillies, J. A., Ishizuka, M., Leys, J. F., et al. (2014). An improved dust emission model – Part 1: Model description and comparison against measurements. *Atmospheric Chemistry and Physics*, *14*(23), 13023–13041. https://doi.org/10.5194/acp-14-13023-2014

Kok, J. F., Parteli, E. J., Michaels, T. I., & Karam, D. B. (2012). The physics of wind-blown sand and dust. *Reports on Progress in Physics*, *75*(10), 106901. https://doi.org/10.1088/0034-4885/75/10/106901

Kumar, P., Sokolik, I. N., & Nenes, A. (2011). Measurements of cloud condensation nuclei activity and droplet activation kinetics of fresh unprocessed regional dust samples and minerals. *Atmospheric Chemistry and Physics*, *11*(7), 3527–3541. https://doi.org/10.5194/acp-11-3527-2011

Lancaster, N., & Baas, A. (1998). Influence of vegetation cover on sand transport by wind: Field studies at owens lake, california. *Earth Surface Processes and Landforms*. (Vol. *23*, pp. 69–82). CO. https://doi.org/10.1002/(SICI)1096-9837(199801)23:1<69

Lareau, N. P., & Clements, C. B. (2017). The Mean and Turbulent Properties of a Wildfire Convective Plume. *Journal of Applied Meteorology and Climatology*, *56*(8), 2289–2299. https://doi.org/10.1175/JAMC-D-16-0384.1

Levin, N., Levental, S., & Morag, H. (2012). The effect of wildfires on vegetation cover and dune activity in Australia's desert dunes: A multisensor analysis. *International Journal of Wildland Fire*, *21*(4), 459–475. https://doi.org/10.1071/WF10150

Liu, Y., Stanturf, J., & Goodrick, S. (2010). Trends in global wildfire potential in a changing climate. *Forest Ecology and Management*, *259*(4), 685–697. https://doi.org/10.1016/j.foreco.2009.09.002

Lu, H., & Shao, Y. (1999). A new model for dust emission by saltation bombardment. *Journal of Geophysical Research*, *104*(D14), 16827–16842. https://doi.org/10.1029/1999JD900169

MacKinnon, D. J., Clow, G. D., Tigges, R. K., Reynolds, R. L., & Chavez, P. (2004). Comparison of aerodynamically and model-derived roughness lengths (z0) over diverse surfaces, central Mojave Desert, California, USA. *Geomorphology*, *63*(1), 103–113. https://doi.org/10.1016/j.geomorph.2004.03.009

Macpherson, T., Nickling, W. G., Gillies, J. A., & Etyemezian, V. (2008). Dust emissions from undisturbed and disturbed supply-limited desert surfaces. *Journal of Geophysical Research: Earth Surface*, *113*(F2), F02S04. https://doi.org/10.1029/2007JF000800

Maenhaut, W., Salma, I., Cafmeyer, J., Annegarn, H. J., & Andreae, M. O. (1996). Regional atmospheric aerosol composition and sources in the eastern Transvaal, South Africa, and impact of biomass burning. *Journal of Geophysical Research*, *101*(D19), 23631–23650. https://doi.org/10.1029/95JD02930

Marticorena, B., & Bergametti, G. (1995). Modeling the atmospheric dust cycle: 1. Design of a soil-derived dust emission scheme. *Journal of Geophysical Research*, *100*(D8), 16415–16430. https://doi.org/10.1029/95JD00690

Marticorena, B., Bergametti, G., Aumont, B., Callot, Y., N'Doumé, C., & Legrand, M. (1997). Modeling the atmospheric dust cycle: 2. Simulation of Saharan dust sources. *Journal of Geophysical Research*, *102*(D4), 4387–4404. https://doi.org/10.1029/96JD02964

McKenna-Neuman, C., & Nickling, W. G. (1989). A theoretical and wind tunnel investigation of the effect of capillary water on the entrainment of sediment by wind. *Canadian Journal of Soil Science*, *69*(1), 79–96. https://doi.org/10.4141/cjss89-008

McNabb, D., & Swanson, F. (1990). Effects of Fire on Soil Erosion. In D. S. JD Walstad SR Radosevich (Ed.), *Natural and prescribed fire in Pacific Northwest forests* (pp. 159–176): Oregon State University Press.

Merino-Martín, L., Field, J. P., Villegas, J. C., Whicker, J. J., Breshears, D. D., Law, D. J., & Urgeghe, A. M. (2014). Aeolian sediment and dust fluxes during predominant "background" wind conditions for unburned and burned semiarid grassland: Interplay between particle size and temporal scale. *Aeolian Research*, *14*, 97–103. https://doi.org/10.1016/j.aeolia.2014.02.004

Neakrase, L., Balme, M., Esposito, F., Kelling, T., Klose, M., Kok, J., et al. (2016). Particle lifting processes in dust devils. *Space Science Reviews*, *203*(1–4), 347–376. https://doi.org/10.1007/s11214-016-0296-6

Nisantzi, A., Mamouri, R. E., Ansmann, A., & Hadjimitsis, D. (2014). Injection of mineral dust into the free troposphere during fire events observed with polarization lidar at Limassol, Cyprus. *Atmospheric Chemistry and Physics*, *14*(22), 12155–12165. https://doi.org/10.5194/acp-14-12155-2014

Owen, P. R. (1964). Saltation of uniform grains in air. *Journal of Fluid Mechanics*, *20*(2), 225–242. https://doi.org/10.1017/s0022112064001173

Palmer, T. Y. (1981). Large fire winds, gases and smoke. *Atmospheric Environment*, *15*(10–11), 2079–2090. https://doi.org/10.1016/0004-6981(81)90241-9

Pérez-Cabello, F., de la Riva Fernández, J., Montorio Llovería, R., & García-Martín, A. (2006). Mapping erosion-sensitive areas after wildfires using fieldwork, remote sensing, and geographic information systems techniques on a regional scale. *Journal of Geophysical Research: Biogeosciences*, *111*(G4), G04S10. https://doi.org/10.1029/2005JG000148

Peterson, D. A., Hyer, E. J., Campbell, J. R., Fromm, M. D., Hair, J. W., Butler, C. F., & Fenn, M. A. (2015). The 2013 Rim fire: Implications for predicting extreme fire spread, pyroconvection, and smoke emissions. *Bulletin of the American Meteorological Society*, *96*(2), 229–247. https://doi.org/10.1175/BAMS-D-14-00060.1

Radke, L. F., Hegg, D. A., Hobbs, P. V., Nance, J. D., Lyons, J. H., Laursen, K. K., & Ward, D. E. (1991). Particulate and trace gas emissions from large biomass fire in North America. *Global biomass burning: Atmospheric, climatic, and biospheric implications* (pp. 209–216): The MIT Press.

Randerson, J. T., Chen, Y., van der Werf, G. R., Rogers, B. M., & Morton, D. C. (2012). Global burned area and biomass burning emissions from small fires. *Journal of Geophysical Research: Biogeosciences*, *117*(G4). https://doi.org/10.1029/2012JG002128

Raupach, M. R., Gillette, D. A., & Leys, J. F. (1993). The effect of roughness elements on wind erosion threshold. *Journal of Geophysical Research*, *98*(D2), 3023–3029. https://doi.org/10.1029/92JD01922

Ravi, S., Baddock, M. C., Zobeck, T. M., & Hartman, J. (2012). Field evidence for differences in post-fire aeolian transport related to vegetation type in semi-arid grasslands. *Aeolian Research*, *7*, 3–10. https://doi.org/10.1016/j.aeolia.2011.12.002

Reid, J. S., Hobbs, P. V., Ferek, R. J., Blake, D. R., Martins, J. V., Dunlap, M. R., & Liousse, C. (1998). Physical, chemical, and optical properties of regional hazes dominated by smoke in Brazil. *Journal of Geophysical Research*, *103*(D24), 32059–32080. https://doi.org/10.1029/98JD00458

Roney, J. A., & White, B. R. (2004). Definition and measurement of dust aeolian thresholds. *Journal of Geophysical Research*, *109*(F1), F01013. https://doi.org/10.1029/2003JF000061

Sanderson, B. M., & Fisher, R. A. (2020). A fiery wake-up call for climate science. *Nature Climate Change*, *10*(3), 175–177. https://doi.org/10.1038/s41558-020-0707-2

Schlosser, J. S., Braun, R. A., Bradley, T., Dadashazar, H., MacDonald, A. B., Aldhaif, A. A., et al. (2017). Analysis of aerosol composition data for western United States wildfires between 2005 and 2015: Dust emissions, chloride depletion, and most enhanced aerosol constituents. *Journal of Geophysical Research: Atmosphere*, *122*(16), 8951–8966. https://doi.org/10.1002/2017JD026547

Shao, Y. (2000). *Physics and modelling of wind erosion*: Kluwer Academic Publishers.

Shao, Y. (2001). A model for mineral dust emission. *Journal of Geophysical Research*, *106*(D17), 20239–20254. https://doi.org/10.1029/2001JD900171

Shao, Y. (2008). *Physics and Modelling of Wind Erosion* (Vol. 37). Springer Science & Business Media.

Shao, Y., & Lu, H. (2000). A simple expression for wind erosion threshold friction velocity. *Journal of Geophysical Research*, *105*(D17), 22437–22443. https://doi.org/10.1029/2000JD900304

Shao, Y., Raupach, M. R., & Findlater, P. A. (1993). Effect of saltation bombardment on the entrainment of dust by wind. *Journal of Geophysical Research*, *98*(D7), 12719–12726. https://doi.org/10.1029/93JD00396

Spiga, A., Barth, E., Gu, Z., Hoffmann, F., Ito, J., Jemmett-Smith, B., et al. (2016). Large-eddy simulations of dust devils and convective vortices. *Space Science Reviews*, *203*(1), 245–275. https://doi.org/10.1007/s11214-016-0284-x

Tegen, I., Harrison, S. P., Kohfeld, K., Prentice, I. C., Coe, M., & Heimann, M. (2002). Impact of vegetation and preferential source areas on global dust aerosol: Results from a model study. *Journal of Geophysical Research*, *107*(D21), 4576. https://doi.org/10.1029/2001JD000963

Tegen, I., & Schepanski, K. (2018). Climate feedback on aerosol emission and atmospheric concentrations. *Current Climate Change Reports*, *4*(1), 1–10. https://doi.org/10.1007/s40641-018-0086-1

Tegen, I., Schepanski, K., & Heinold, B. (2013). Comparing two years of Saharan dust source activation obtained by regional modelling and satellite observations. *Atmospheric Chemistry and Physics*, *13*, 2381–2390. https://doi.org/10.5194/acp-13-2381-2013

Vermeire, L. T., Wester, D. B., Mitchell, R. B., & Fuhlendorf, S. D. (2005). Fire and grazing effects on wind erosion, soil water content, and soil temperature. *Journal of Environmental Quality*, *34*(5), 1559–1565. https://doi.org/10.2134/jeq2005.0006

Wagner, R. (2021). Data related to Wagner et al. (2021, JGR): "The dust emission potential of agricultural-like fires - Theoretical estimates from two conceptually different dust emission parameterizations". *Zenodo*. https://doi.org/10.5281/zenodo.5205676

Wagner, R., Jähn, M., & Schepanski, K. (2018). Wildfires as a source of airborne mineral dust – Revisiting a conceptual model using large-eddy simulation (LES). *Atmospheric Chemistry and Physics*, *18*(16), 11863–11884. https://doi.org/10.5194/acp-18-11863-2018

Westerling, A. (2006). Increasing western US forest wildfire activity: Sensitivity to changes in the timing of spring. *Philosophical Transactions of the Royal Society B*, *371*(1696), 20150178. https://doi.org/10.1098/rstb.2015.0178

Westerling, A., & Bryant, B. (2008). Climate change and wildfire in California. *Climatic Change*, *87*(1), 231–249. https://doi.org/10.1007/s10584-007-9363-z

Whicker, J. J., Pinder, J. E., & Breshears, D. D. (2006). Increased wind erosion from forest wildfire: Implications for contaminant-related risks. *Journal of Environmental Quality*, *35*(2), 468–478. https://doi.org/10.2134/jeq2005.0112

Wolfe, S. A. & Nickling, W. G. (1996). Shear stress partitioning in sparsely vegetated desert canopies. *Earth Surface Processes and Landforms*, *21*(7), 607–619. https://doi.org/10.1002/(SICI)1096-9837(199607)21:7<607::AID-ESP660>3.0.CO;2-1

Wu, C., Lin, Z., & Liu, X. (2020). The global dust cycle and uncertainty in CMIP5 (Coupled Model Intercomparison Project phase 5) models. *Atmospheric Chemistry and Physics*, *20*(17), 10401–10425. https://doi.org/10.5194/acp-20-10401-2020

Zhang, J., Teng, Z., Huang, N., Guo, L., & Shao, Y. (2016). Surface renewal as a significant mechanism for dust emission. *Atmospheric Chemistry and Physics*, *16*(24), 15517–15528. https://doi.org/10.5194/acp-16-15517-2016

Zimon, A. D. (1982). *Adhesion of dust and powder* (pp. 241–270). Springer. https://doi.org/10.1007/978-1-4615-8576-3_8